Design of 3-RPS Parallel Manipulators based on Operation Modes

Latifah Nurahmi, Stéphane Caro, Philippe Wenger

Design of 3-RPS Parallel Manipulators based on Operation Modes

Latifah Nurahmi, Stéphane Caro, Philippe Wenger
Institut de Recherche en Communications et Cybernétique de Nantes,
Emails: {latifah.nurahmi, stephane.caro, philippe.wenger}@irccyn.ec-nantes.fr

Abstract— *The subject of this paper is about the synthesis of the design parameters of a parallel manipulator with three RPS legs while considering the prescribed operation modes at the design stage. The synthesis is based on the Euler parametrization and the results of primary decomposition. The design parameters and the coordinates of one RPS leg are initially defined to formulate the constraint equation associated with this leg. Seven classes of RPS legs are identified and the geometric properties of each class are highlighted. By selecting three different or identical classes of the RPS leg, a new 3-RPS parallel manipulator is proposed without specific values of the design parameters. The primary decomposition is computed over a set of three constraint equations. One or more Euler parameter(s) in the results of primary decomposition is(are) constrained to be equal to zero, which leads to particular types of operation modes. The methodology also provides new architectures of the 3-RPS parallel manipulators based on a classification of the RPS legs, that satisfy the prescribed operation mode.*

Keywords: Synthesis, design parameters, primary decomposition, operation mode, RPS legs

I. Introduction

The well-known 3-RPS (R, P, S, represent revolute, prismatic, and spherical joints, respectively) parallel manipulator with different shapes for the moving platform and the base was extensively studied by many researchers. In 1983 [1], Hunt introduced the 3-RPS manipulator which has an equilateral triangle base and an equilateral triangle platform. Since then, many researches and experimentations have been presented to deal with this manipulator. Huang *et al.* in [2] examined the principal screws of the 3-RPS manipulator in several configurations. Tsai [3] and Schadlbauer *et al.* [4] used different approaches to enumerate sixteen solutions of the direct kinematics. Schadlbauer *et al.* also revealed that the 3-RPS manipulator has two distinct operation modes. Later in [5], Schadlbauer *et al.* characterized the motion type in both operation modes by using the axodes. The self-motions of this mechanism were classified in [6] via Study kinematic mapping.

Kim *et al.* in [7] determined the design parameters of the 3-RPS manipulator to fulfil six prescribed positions of the moving platform. However in most of the cases six precision point accuracy is not sufficient to obtain a given motion. Hence Rao *et al.* [8] modified the synthesis method by means of the least square method and the Newton-Raphson method to synthesize the design parameters for any number of approximate prescribed positions of the moving platform. Later in [9], Rao *et al.* improved the approximation results by adopting the Genetic Algorithm.

Another parallel manipulator of the 3-RPS family is the 3-RPS cube manipulator and was proposed by Huang *et al.* in 1995 [10]. The 3-RPS cube manipulator is composed of a cube-shaped base and an equilateral triangle platform. Huang *et al.* in 2011 [11] discussed the impact of manufacturing errors and the orientation capability based on the Euler angles for a group of *3-dof* rotational parallel mechanisms without intersecting axes. The following year the type synthesis of this motion group was presented in [12].

By identifying the reciprocal screws of each leg, Huang *et al.* in [13] showed that the 3-RPS cube manipulator is able to perform *1-dof* motion along its diagonal, which is known as the Vertical Darboux Motion. This phenomenon was further discussed by Nurahmi *et al.* in [14], [15], [16], using the Study kinematic mapping. The authors also found that this mechanism has only one operation mode in which the *3-dof* general motion and the Vertical Darboux Motion occur inside the same operation mode.

Bai *et al.* in [17] studied the kinematics of the 3-PPR planar parallel manipulator with different types of the base and the platform. The authors also designed a novel planar parallel robot with a non-symmetrical base which is able to perform large workspace without affecting its motion accuracy.

The 3-RPS manipulator proposed by Hunt and the 3-RPS cube manipulator proposed by Huang have three identical RPS legs. However, the number and the types of operation modes for both manipulators are different due to the manipulator architectures. The axes of the three revolute joints in the 3-RPS cube manipulator are orthogonal to each other, while the axes of the three revolute joints in the 3-RPS manipulator proposed by Hunt are coplanar.

Accordingly, a general approach to synthesize the design parameters by considering the prescribed operation modes for a parallel manipulator with three RPS legs, is discussed in more details in this paper. The approach is based on the Euler parametrization [18], and the primary decomposition is used to reveal the existence of the number and the type of operation modes [19]-[22].

The first essential step is to characterize the coordinates and to define the design parameters of one RPS leg. Then, the

constraint equation of this RPS leg is formulated by means of the Euler parametrization. This constraint equation should vanish in any configuration of the moving platform, likewise in the home configuration where the fixed frame and the moving frame are coincident. As a result, seven classes of the RPS legs are obtained based on the position and the orientation of the RPS legs.

By selecting three different or identical classes of the RPS legs, 3-RPS parallel manipulators are obtained without any specific value of the design parameters. This is an intermediate stage and one needs to derive the constraint equations of the corresponding new manipulator and compute the primary decomposition. In the results of primary decomposition, one or more Euler parameter(s) is(are) constrained to be null. Under this condition, the design parameters are synthesized.

This paper is organized as follows: A detailed definition of the design parameters is given in Section 2. The constraint equation of one RPS leg is expressed in Section 3. This equation is used to classify seven classes of the RPS legs in Section 4. Eventually in Section 5, some new 3-RPS parallel manipulators are synthesized by selecting three identical classes for the RPS legs corresponding to the prescribed operation modes.

II. Parametrization of the RPS Leg

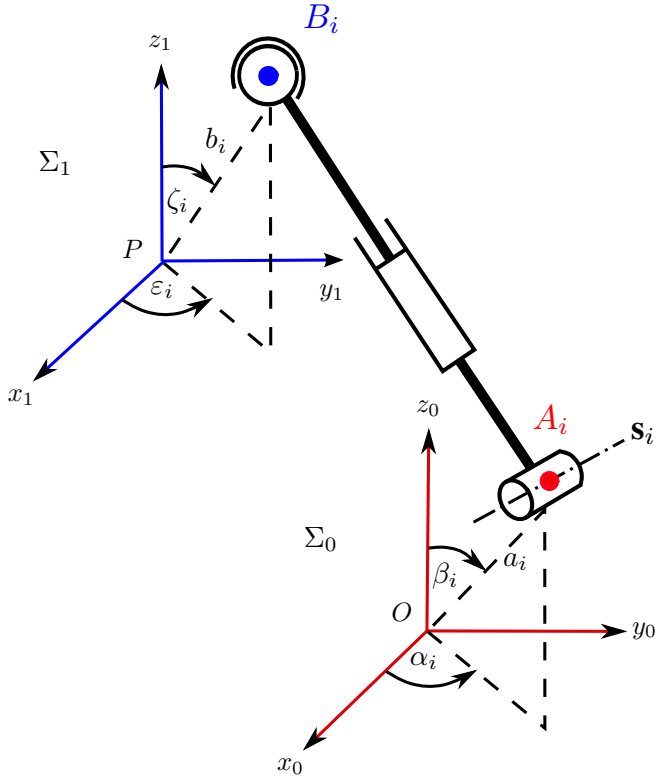

Fig. 1. Parameters of the RPS leg.

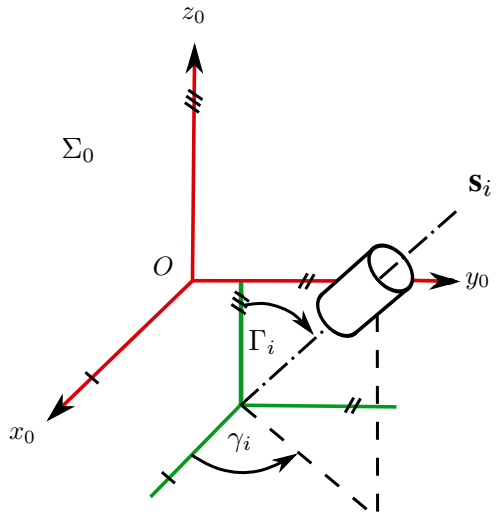

Fig. 2. The axis of revolute joint.

The RPS leg depicted in Fig. 1, is composed of a revolute joint, an actuated prismatic joint, and a spherical joint mounted in series. The revolute joint is attached to the base and denoted by point A_i (i denotes the number of the leg used in the manipulator, $i = 1, 2, 3$). This point is located in the three-dimensional space which is specified by the azimuth angle α_i, the polar angle β_i, and the radial distance a_i from the origin O of the fixed frame Σ_0.

The spherical joint is attached to the moving platform and denoted by point B_i. This point is also located in the three-dimensional space which is specified by the azimuth angle ε_i, the polar angle ζ_i, and the radial distance b_i from the origin P of the moving frame Σ_1. The axis of the revolute joint is along the vector $\mathbf{s}_i$, which is specified by the azimuth angle γ_i and the polar angle Γ_i (Fig. 2). The coordinates of points A_i, B_i and unit vector $\mathbf{s}_i$ are:

$$\begin{aligned} \mathbf{r}^0_{A_i} &= \begin{bmatrix} 1, & c_{\alpha_i} c_{\beta_i} a_i, & s_{\alpha_i} c_{\beta_i} a_i, & s_{\beta_i} a_i \end{bmatrix}^T, \\ \mathbf{r}^1_{B_i} &= \begin{bmatrix} 1, & c_{\varepsilon_i} c_{\zeta_i} b_i, & s_{\varepsilon_i} c_{\zeta_i} b_i, & s_{\zeta_i} b_i \end{bmatrix}^T, \\ \mathbf{s}_i &= \begin{bmatrix} 0, & c_{\gamma_i} c_{\Gamma_i}, & s_{\gamma_i} c_{\Gamma_i}, & s_{\Gamma_i} \end{bmatrix}^T. \end{aligned} \tag{1}$$

where $c_{\alpha_i} = \cos(\alpha_i), s_{\alpha_i} = \sin(\alpha_i), c_{\beta_i} = \cos(\beta_i), s_{\beta_i} = \sin(\beta_i), c_{\varepsilon_i} = \cos(\varepsilon_i), s_{\varepsilon_i} = \sin(\varepsilon_i), c_{\zeta_i} = \cos(\zeta_i), s_{\zeta_i} = \sin(\zeta_i), c_{\gamma_i} = \cos(\gamma), s_{\gamma_i} = \sin(\gamma), c_{\Gamma_i} = \cos(\Gamma)$, and $s_{\Gamma_i} = \sin(\Gamma)$. As a consequence, there are eight design parameters for one RPS leg, namely a_i, b_i, α_i, β_i, ε_i, ζ_i, γ_i, and Γ_i. Since the 3-RPS parallel manipulator is composed of three legs, it has 24 design parameters.

III. Leg Constraint Equation

In this section, the constraint equation is expressed for one RPS leg shown in Fig. 1. To obtain the coordinates of point B_i expressed in the fixed frame Σ_0, the transformation matrix $\mathbf{M}$ is used as follows:

$$\mathbf{M} = \begin{pmatrix} x_0^2 + x_1^2 + x_2^2 + x_3^2 & \mathbf{0}_{3\times 1}^T \\ \mathbf{d} & \mathbf{R} \end{pmatrix} \tag{2}$$

$\mathbf{R}$ is an orthogonal matrix obtained with the Euler parametrization [18] and $\mathbf{d}$ is the point-displacement vector:

$$\mathbf{R} = \begin{pmatrix} x_0^2 + x_1^2 - x_2^2 - x_3^2 & 2(x_1x_2 - x_0x_3) & 2(x_1x_3 + x_0x_2) \\ 2(x_1x_2 + x_0x_3) & x_0^2 - x_1^2 + x_2^2 - x_3^2 & 2(x_2x_3 - x_0x_1) \\ 2(x_1x_3 - x_0x_2) & 2(x_2x_3 + x_0x_1) & x_0^2 - x_1^2 - x_2^2 + x_3^2 \end{pmatrix}$$
$$\mathbf{d} = \begin{pmatrix} X \\ Y \\ Z \end{pmatrix} \tag{3}$$

The parameters x_0, x_1, x_2, x_3, which appear in matrix $\mathbf{R}$, are called Euler parameters of the rotation. They are useful in the representation of a spatial Euclidean displacement and should satisfy the following equation [24]:

$$x_0^2 + x_1^2 + x_2^2 + x_3^2 - 1 = 0 \tag{4}$$

This condition will be used in the following computations to simplify the algebraic expressions. The coordinates of point B_i expressed in Σ_0 are obtained by:

$$\mathbf{r}_{B_i}^0 = \mathbf{M}\, \mathbf{r}_{B_i}^1 \tag{5}$$

As the coordinates of all points are given in terms of Euler parameters and design parameters, the constraint equation can be obtained by examining the design of the RPS leg. The leg connecting points A_i and B_i is orthogonal to the axis $\mathbf{s}_i$ of the revolute joint. Accordingly, the scalar product of vector $(\mathbf{r}_{B_i}^0 - \mathbf{r}_{A_i}^0)$ and vector $\mathbf{s}_i$ vanishes, namely:

$$(\mathbf{r}_{B_i}^0 - \mathbf{r}_{A_i}^0)^T\, \mathbf{s}_i = 0 \tag{6}$$

After computing the corresponding scalar product and removing the common denominators, the following constraint equation of one RPS leg comes out:

$$\begin{aligned} h_i : {} & c_{\gamma_i}c_{\Gamma_i}X + c_{\Gamma_i}s_{\gamma_i}Y + (x_0^2 - x_1^2 - x_2^2 + x_3^2)s_{\zeta_i}s_{\Gamma_i}b_i \\ & - s_{\beta_i}s_{\Gamma_i}a_i + (2x_1x_2 - 2x_0x_3)b_ic_{\Gamma_i}c_{\gamma_i}s_{\varepsilon_i}c_{\zeta_i} + (2 \\ & x_0x_3 + 2x_1x_2)b_is_{\gamma_i}c_{\Gamma_i}c_{\zeta_i}c_{\varepsilon_i} + (x_0^2 + x_1^2 - x_2^2 - x_3^2) \\ & c_{\varepsilon_i}c_{\zeta_i}c_{\gamma_i}c_{\Gamma_i}b_i - c_{\alpha_i}c_{\beta_i}c_{\gamma_i}c_{\Gamma_i}a_i + (x_0^2 - x_1^2 + x_2^2 - \\ & x_3^2)c_{\zeta_i}s_{\varepsilon_i}c_{\Gamma_i}s_{\gamma_i}b_i - c_{\beta_i}c_{\Gamma_i}s_{\alpha_i}s_{\gamma_i}a_i + (2x_0x_1 + 2x_2 \\ & x_3)b_is_{\Gamma_i}s_{\varepsilon_i}c_{\zeta_i} + (2x_0x_2 + 2x_1x_3)b_ic_{\Gamma_i}c_{\gamma_i}s_{\zeta_i} + (2 \\ & x_2x_3 - 2x_0x_1)b_is_{\gamma_i}c_{\Gamma_i}s_{\zeta_i} + (2x_1x_3 - 2x_0x_2)b_is_{\Gamma_i} \\ & c_{\zeta_i}c_{\varepsilon_i} + s_{\Gamma_i}Z = 0 \end{aligned} \tag{7}$$

IV. Classification of the RPS legs

In this section, the constraint equation associated with the design parameters are solved to synthesize seven classes of RPS legs. The constraint equations h_i $(i = 1, 2, 3)$ in Eq. (7) should vanish for any configuration of the moving platform and in particular in the home configuration where the fixed frame and the moving frame coincide. In the home configuration, the transformation matrix $\mathbf{M}$ defined by Eq. (2) becomes the identity matrix $\mathbf{I}$ and the variables become $x_0 = 1, x_1 = 0, x_2 = 0, x_3 = 0, X = 0, Y = 0, Z = 0$. By substituting these values into Eq. (7), h_i takes the following form:

$$\begin{aligned} h_i^0 : {} & (c_{\varepsilon_i}c_{\zeta_i}c_{\gamma_i}c_{\Gamma_i} + c_{\zeta_i}c_{\Gamma_i}s_{\varepsilon_i}s_{\gamma_i} + s_{\zeta_i}s_{\Gamma_i})b_i - \\ & (c_{\alpha_i}c_{\beta_i}c_{\gamma_i}c_{\Gamma_i} + c_{\beta_i}c_{\Gamma_i}s_{\alpha_i}s_{\gamma_i} + s_{\beta_i}s_{\Gamma_i})a_i = 0 \end{aligned} \tag{8}$$

Equation (8) does not bring any geometric insight on the geometric arrangements of the 3-RPS legs for the 3-RPS parallel manipulator to be assembled in the home configuration. As a consequence, we are looking for some particular geometric arrangements of the legs for the 3-RPS parallel manipulator to be assembled. For instance, the manipulator can be assembled in the home configuration when the two following terms vanish:

$$\begin{aligned} m_i = {} & (c_{\varepsilon_i}c_{\zeta_i}c_{\gamma_i}c_{\Gamma_i} + c_{\zeta_i}c_{\Gamma_i}s_{\varepsilon_i}s_{\gamma_i} + s_{\zeta_i}s_{\Gamma_i})b_i \\ n_i = {} & (c_{\alpha_i}c_{\beta_i}c_{\gamma_i}c_{\Gamma_i} + c_{\beta_i}c_{\Gamma_i}s_{\alpha_i}s_{\gamma_i} + s_{\beta_i}s_{\Gamma_i})a_i \end{aligned}$$

with:

$$h_i^0 : m_i - n_i = 0 \tag{9}$$

It can be seen that m_i and n_i are polynomials in terms of the design parameters. To find the relations between the design parameters for which the constraint equation h_i^0 vanishes, we compute one particular condition where m_i and n_i vanish simultaneously. One has to discuss the ideal $\mathcal{I} = \langle m_i, n_i \rangle$ and compute the Groebner basis with lexicographic order. Twenty three relations are obtained and substituted into Eq. (1). For detailed results of the 23 relations, the reader can refer to [23].

Based on their geometric properties, seven classes are identified and each class contains one or more sub-classes as shown in Table I. The detailed expressions of each sub-class are presented in Table II-IV. The sub-classes give the location of the RPS legs in the three-dimensional space, in which $\mathbf{r}_{A_i}^0$ gives the location of the revolute joint with respect to Σ_0, $\mathbf{r}_{B_i}^1$ gives the location of the spherical joint with respect to Σ_1, and $\mathbf{s}_i$ gives the unit vector of the axis of the revolute joint with respect to Σ_0.

By selecting three different or identical classes, a new manipulator with three RPS legs can be created. The user may assign some arbitrary values into the design parameters and assemble the legs accordingly. However, it is interesting to

Class	Sub-class	Geometric properties
A	A.1	Points A_i, B_i are located at the origins of Σ_0 and Σ_1, respectively; the axes of R-joints are arbitrary
B	B.1, B.2	Points A_i, B_i are located in the **xy**-plane of Σ_0 and Σ_1, respectively; the axes of R-joints are parallel to the **z**-axis
C	C.1, C.2, C.3, C.4	Points A_i, B_i are located on the **z**-axis of Σ_0 and Σ_1, respectively; the axes of R-joints are parallel to the **xy**-plane of Σ_0
D	D.1, D.2, D.3, D.4	Point A_i is located on **z**-axis of Σ_0 and point B_i is located in any position in Σ_1; the axes of R-joints are parallel to the **xy**-plane of Σ_0
E	E.1, E.2, E.3, E.4	Point A_i is located in any position in Σ_0 and point B_i is located on the **z**-axis of Σ_1; the axes of R-joints are parallel to the **xy**-plane of Σ_0
F	F.1, F.2, F.3, F.4	Points A_i, B_i are located in any position in Σ_0 and Σ_1, respectively; the axes of R-joints are parallel to the **xy**-plane of Σ_0
G	G.1, G.2, G.3, G.4	Points A_i, B_i are located in the **xy**-plane of Σ_0 and Σ_1, respectively; the axes of R-joints can take any orientation

TABLE I. Classes and Sub-classes of RPS Legs

generate various designs of the 3-RPS manipulator that fulfil the prescribed operation modes as presented in the following.

V. Synthesis of Design Parameters

In the following, an example of 3-RPS parallel manipulator with three identical classes of the RPS leg is presented. Then, the design parameters associated with the new manipulator are synthesized by imposing the prescribed operation modes.

Class	Sub-class	Coordinates of points and axis		
		$\mathbf{r}^0_{A_i}$	$\mathbf{r}^1_{B_i}$	$\mathbf{s}_i$
A	A.1	$\begin{bmatrix}1\\0\\0\\0\end{bmatrix}$	$\begin{bmatrix}1\\0\\0\\0\end{bmatrix}$	$\begin{bmatrix}0\\c_{\gamma_i}c_{\Gamma_i}\\s_{\gamma_i}c_{\Gamma_i}\\s_{\Gamma_i}\end{bmatrix}$
B	B.1	$\begin{bmatrix}1\\c_{\alpha_i}a_i\\s_{\alpha_i}a_i\\0\end{bmatrix}$	$\begin{bmatrix}1\\c_{\varepsilon_i}b_i\\s_{\varepsilon_i}b_i\\0\end{bmatrix}$	$\begin{bmatrix}0\\0\\0\\1\end{bmatrix}$
	B.2	$\begin{bmatrix}1\\c_{\alpha_i}a_i\\s_{\alpha_i}a_i\\0\end{bmatrix}$	$\begin{bmatrix}1\\c_{\varepsilon_i}b_i\\s_{\varepsilon_i}b_i\\0\end{bmatrix}$	$\begin{bmatrix}0\\0\\0\\-1\end{bmatrix}$
C	C.1	$\begin{bmatrix}1\\0\\0\\a_i\end{bmatrix}$	$\begin{bmatrix}1\\0\\0\\b_i\end{bmatrix}$	$\begin{bmatrix}0\\c_{\gamma_i}\\s_{\gamma_i}\\0\end{bmatrix}$
	C.2	$\begin{bmatrix}1\\0\\0\\a_i\end{bmatrix}$	$\begin{bmatrix}1\\0\\0\\-b_i\end{bmatrix}$	$\begin{bmatrix}0\\c_{\gamma_i}\\s_{\gamma_i}\\0\end{bmatrix}$
	C.3	$\begin{bmatrix}1\\0\\0\\-a_i\end{bmatrix}$	$\begin{bmatrix}1\\0\\0\\b_i\end{bmatrix}$	$\begin{bmatrix}0\\c_{\gamma_i}\\s_{\gamma_i}\\0\end{bmatrix}$
	C.4	$\begin{bmatrix}1\\0\\0\\-a_i\end{bmatrix}$	$\begin{bmatrix}1\\0\\0\\-b_i\end{bmatrix}$	$\begin{bmatrix}0\\c_{\gamma_i}\\s_{\gamma_i}\\0\end{bmatrix}$
D	D.1	$\begin{bmatrix}1\\0\\0\\a_i\end{bmatrix}$	$\begin{bmatrix}1\\-s_{\gamma_i}c_{\zeta_i}b_i\\c_{\gamma_i}c_{\zeta_i}b_i\\s_{\zeta_i}b_i\end{bmatrix}$	$\begin{bmatrix}0\\c_{\gamma_i}\\s_{\gamma_i}\\0\end{bmatrix}$
	D.2	$\begin{bmatrix}1\\0\\0\\a_i\end{bmatrix}$	$\begin{bmatrix}1\\s_{\gamma_i}c_{\zeta_i}b_i\\-c_{\gamma_i}c_{\zeta_i}b_i\\s_{\zeta_i}b_i\end{bmatrix}$	$\begin{bmatrix}0\\c_{\gamma_i}\\s_{\gamma_i}\\0\end{bmatrix}$
	D.3	$\begin{bmatrix}1\\0\\0\\-a_i\end{bmatrix}$	$\begin{bmatrix}1\\-s_{\gamma_i}c_{\zeta_i}b_i\\c_{\gamma_i}c_{\zeta_i}b_i\\s_{\zeta_i}b_i\end{bmatrix}$	$\begin{bmatrix}0\\c_{\gamma_i}\\s_{\gamma_i}\\0\end{bmatrix}$

TABLE II. Coordinates of points A_i and B_i and revolute joint axis for each sub-class

Class	Sub-class	Coordinates of points and axis		
		$\mathbf{r}^0_{A_i}$	$\mathbf{r}^1_{B_i}$	$\mathbf{s}_i$
D	D.4	$\begin{bmatrix} 1 \\ 0 \\ 0 \\ -a_i \end{bmatrix}$	$\begin{bmatrix} 1 \\ s_{\gamma_i} c_{\zeta_i} b_i \\ -c_{\gamma_i} c_{\zeta_i} b_i \\ s_{\zeta_i} b_i \end{bmatrix}$	$\begin{bmatrix} 0 \\ c_{\gamma_i} \\ s_{\gamma_i} \\ 0 \end{bmatrix}$
E	E.1	$\begin{bmatrix} 1 \\ -s_{\gamma_i} c_{\beta_i} a_i \\ c_{\gamma_i} c_{\beta_i} a_i \\ s_{\beta_i} a_i \end{bmatrix}$	$\begin{bmatrix} 1 \\ 0 \\ 0 \\ b_i \end{bmatrix}$	$\begin{bmatrix} 0 \\ c_{\gamma_i} \\ s_{\gamma_i} \\ 0 \end{bmatrix}$
	E.2	$\begin{bmatrix} 1 \\ s_{\gamma_i} c_{\beta_i} a_i \\ -c_{\gamma_i} c_{\beta_i} a_i \\ s_{\beta_i} a_i \end{bmatrix}$	$\begin{bmatrix} 1 \\ 0 \\ 0 \\ b_i \end{bmatrix}$	$\begin{bmatrix} 0 \\ c_{\gamma_i} \\ s_{\gamma_i} \\ 0 \end{bmatrix}$
	E.3	$\begin{bmatrix} 1 \\ -s_{\gamma_i} c_{\beta_i} a_i \\ c_{\gamma_i} c_{\beta_i} a_i \\ s_{\beta_i} a_i \end{bmatrix}$	$\begin{bmatrix} 1 \\ 0 \\ 0 \\ -b_i \end{bmatrix}$	$\begin{bmatrix} 0 \\ c_{\gamma_i} \\ s_{\gamma_i} \\ 0 \end{bmatrix}$
	E.4	$\begin{bmatrix} 1 \\ s_{\gamma_i} c_{\beta_i} a_i \\ -c_{\gamma_i} c_{\beta_i} a_i \\ s_{\beta_i} a_i \end{bmatrix}$	$\begin{bmatrix} 1 \\ 0 \\ 0 \\ -b_i \end{bmatrix}$	$\begin{bmatrix} 0 \\ c_{\gamma_i} \\ s_{\gamma_i} \\ 0 \end{bmatrix}$
F	F.1	$\begin{bmatrix} 1 \\ -s_{\gamma_i} c_{\beta_i} a_i \\ c_{\gamma_i} c_{\beta_i} a_i \\ s_{\beta_i} a_i \end{bmatrix}$	$\begin{bmatrix} 1 \\ -s_{\gamma_i} c_{\zeta_i} b_i \\ c_{\gamma_i} c_{\zeta_i} b_i \\ s_{\zeta_i} b_i \end{bmatrix}$	$\begin{bmatrix} 0 \\ c_{\gamma_i} \\ s_{\gamma_i} \\ 0 \end{bmatrix}$
	F.2	$\begin{bmatrix} 1 \\ c_{\varepsilon_i} c_{\beta_i} a_i \\ s_{\varepsilon_i} c_{\beta_i} a_i \\ s_{\beta_i} a_i \end{bmatrix}$	$\begin{bmatrix} 1 \\ c_{\varepsilon_i} c_{\zeta_i} b_i \\ s_{\varepsilon_i} c_{\zeta_i} b_i \\ s_{\zeta_i} b_i \end{bmatrix}$	$\begin{bmatrix} 0 \\ -s_{\varepsilon_i} \\ c_{\varepsilon_i} \\ 0 \end{bmatrix}$
	F.3	$\begin{bmatrix} 1 \\ -s_{\gamma_i} c_{\beta_i} a_i \\ c_{\gamma_i} c_{\beta_i} a_i \\ s_{\beta_i} a_i \end{bmatrix}$	$\begin{bmatrix} 1 \\ s_{\gamma_i} c_{\zeta_i} b_i \\ -c_{\gamma_i} c_{\zeta_i} b_i \\ s_{\zeta_i} b_i \end{bmatrix}$	$\begin{bmatrix} 0 \\ c_{\gamma_i} \\ s_{\gamma_i} \\ 0 \end{bmatrix}$
	F.4	$\begin{bmatrix} 1 \\ s_{\gamma_i} c_{\beta_i} a_i \\ -c_{\gamma_i} c_{\beta_i} a_i \\ s_{\beta_i} a_i \end{bmatrix}$	$\begin{bmatrix} 1 \\ -s_{\gamma_i} c_{\zeta_i} b_i \\ c_{\gamma_i} c_{\zeta_i} b_i \\ s_{\zeta_i} b_i \end{bmatrix}$	$\begin{bmatrix} 0 \\ c_{\gamma_i} \\ s_{\gamma_i} \\ 0 \end{bmatrix}$
G	G.1	$\begin{bmatrix} 1 \\ -s_{\gamma_i} a_i \\ c_{\gamma_i} a_i \\ 0 \end{bmatrix}$	$\begin{bmatrix} 1 \\ -s_{\gamma_i} b_i \\ c_{\gamma_i} b_i \\ 0 \end{bmatrix}$	$\begin{bmatrix} 0 \\ c_{\gamma_i} c_{\Gamma_i} \\ s_{\gamma_i} c_{\Gamma_i} \\ s_{\Gamma_i} \end{bmatrix}$

TABLE III. Coordinates of points A_i and B_i and revolute joint axis for each sub-class (continued)

Class	Sub-class	Coordinates of points and axis		
		$\mathbf{r}^0_{A_i}$	$\mathbf{r}^1_{B_i}$	$\mathbf{s}_i$
G	G.2	$\begin{bmatrix} 1 \\ s_{\gamma_i} a_i \\ -c_{\gamma_i} a_i \\ 0 \end{bmatrix}$	$\begin{bmatrix} 1 \\ s_{\gamma_i} b_i \\ -c_{\gamma_i} b_i \\ 0 \end{bmatrix}$	$\begin{bmatrix} 0 \\ c_{\gamma_i} c_{\Gamma_i} \\ s_{\gamma_i} c_{\Gamma_i} \\ s_{\Gamma_i} \end{bmatrix}$
	G.3	$\begin{bmatrix} 1 \\ s_{\gamma_i} a_i \\ -c_{\gamma_i} a_i \\ 0 \end{bmatrix}$	$\begin{bmatrix} 1 \\ -s_{\gamma_i} b_i \\ c_{\gamma_i} b_i \\ 0 \end{bmatrix}$	$\begin{bmatrix} 0 \\ c_{\gamma_i} c_{\Gamma_i} \\ s_{\gamma_i} c_{\Gamma_i} \\ s_{\Gamma_i} \end{bmatrix}$
	G.4	$\begin{bmatrix} 1 \\ -s_{\gamma_i} a_i \\ c_{\gamma_i} a_i \\ 0 \end{bmatrix}$	$\begin{bmatrix} 1 \\ s_{\gamma_i} b_i \\ -c_{\gamma_i} b_i \\ 0 \end{bmatrix}$	$\begin{bmatrix} 0 \\ c_{\gamma_i} c_{\Gamma_i} \\ s_{\gamma_i} c_{\Gamma_i} \\ s_{\Gamma_i} \end{bmatrix}$

TABLE IV. Coordinates of points A_i and B_i and revolute joint axis for each sub-class (continued)

A. *Sub-class F.2*

In this section, the 3-RPS manipulator is generated by selecting three identical sub-classes, namely sub-class F.2. The RPS leg in this class consists of a revolute joint and a spherical joint that are located in any position with respect to Σ_0 and Σ_1, respectively. The axis of the revolute joint is parallel to the **xy**-plane of Σ_0. In this sub-class, the coordinates of points A_i, B_i, and vector $\mathbf{s}_i$ are:

$$\begin{aligned} \mathbf{r}^0_{A_i} &= \begin{bmatrix} 1 & c_{\varepsilon_i} c_{\beta_i} a_i & s_{\varepsilon_i} c_{\beta_i} a_i & s_{\beta_i} a_i \end{bmatrix}, \\ \mathbf{r}^1_{B_i} &= \begin{bmatrix} 1 & c_{\varepsilon_i} c_{\zeta_i} b_i & s_{\varepsilon_i} c_{\zeta_i} b_i & s_{\zeta_i} b_i \end{bmatrix}, \\ \mathbf{s}_i &= \begin{bmatrix} 0 & -s_{\varepsilon_i} & c_{\varepsilon_i} & 0 \end{bmatrix}. \end{aligned} \tag{10}$$

Due to the fact that the computation of primary decomposition in software *Singular* fails for reasons of memory and time, points A_i and B_i are assumed to lie in the **xy**-plane of Σ_0 and Σ_1, respectively. Therefore, some values are assigned for $\beta_1 = \beta_2 = \beta_3 = 0$ and $\zeta_1 = \zeta_2 = \zeta_3 = 0$, we obtain:

$$\begin{aligned} \mathbf{r}^0_{A_i} &= \begin{bmatrix} 1 & c_{\varepsilon_i} a_i & s_{\varepsilon_i} a_i & 0 \end{bmatrix}, \\ \mathbf{r}^1_{B_i} &= \begin{bmatrix} 1 & c_{\varepsilon_i} b_i & s_{\varepsilon_i} b_i & 0 \end{bmatrix}. \end{aligned} \tag{11}$$

The first RPS leg of the manipulator is fixed by substituting $\varepsilon_1 = 0$, hence the coordinates of points A_1, B_1 and vector $\mathbf{s}_1$ become:

$$\mathbf{r}^0_{A_1} = \begin{bmatrix} 1 & a_1 & 0 & 0 \end{bmatrix},$$
$$\mathbf{r}^1_{B_1} = \begin{bmatrix} 1 & b_1 & 0 & 0 \end{bmatrix}, \quad (12)$$
$$\mathbf{s}_1 = \begin{bmatrix} 0 & 0 & 1 & 0 \end{bmatrix}.$$

To obtain the coordinates of points B_1, B_2, B_3 expressed in Σ_0, the coordinate transformation is performed by means of the Euler parametrization as stated in Eq. (5), namely $\mathbf{r}^0_{B_i} = \mathbf{M}\,\mathbf{r}^1_{B_i}$ $(i = 1, 2, 3)$.

The constraint equations are determined by computing the scalar products of the vector $\overrightarrow{A_iB_i}$ and the unit vector $\mathbf{s}_i$, which should vanish as stated in Eq. (6), namely $(\mathbf{r}^0_{B_i} - \mathbf{r}^0_{A_i})^T\,\mathbf{s}_i = 0$. The constraint equations take the form:

$$\begin{aligned}
&h_1 : Y + (2x_0x_3 + 2x_1x_2)b_1 = 0\\
&h_2 : 4c^2_{\varepsilon_2}b_2x_1x_2 - 2(x_1^2 - x_2^2)c_{\varepsilon_2}s_{\varepsilon_2}b_2 + c_{\varepsilon_2}Y - s_{\varepsilon_2}X + \\
&\quad (2x_0x_3 - 2x_1x_2)b_2 = 0\\
&h_3 : 4c^2_{\varepsilon_3}b_3x_1x_2 - 2(x_1^2 - x_2^2)c_{\varepsilon_3}s_{\varepsilon_3}b_3 + c_{\varepsilon_3}Y - s_{\varepsilon_3}X + \\
&\quad (2x_0x_3 - 2x_1x_2)b_3 = 0
\end{aligned} \quad (13)$$

For the algebraic computation, the half-tangent substitutions are performed to remove the trigonometric functions in the second and the third legs:

$$s_{\varepsilon_i} = \frac{(2te_i)}{(1 + te_i^2)}, \quad c_{\varepsilon_i} = \frac{(1 - te_i^2)}{(1 + te_i^2)} \quad (14)$$

where $te_i = \tan(\frac{\varepsilon_i}{2})$. Hence, new constraint equations in terms of half-tangents are obtained:

$$\begin{aligned}
&h_1 : Y + (2x_0x_3 + 2x_1x_2)b_1 = 0\\
&h_2 : -2Xte_2^3 - 2te_2X - Yte_2^4 + Y + (2x_0x_3 + 2x_1x_2)\\
&\quad b_2te_2^4 + 4(x_1^2 - x_2^2)b_2te_2^3 + (4x_0x_3 - 12x_1x_2)b_2te_2^2\\
&\quad - 4(x_1^2 - x_2^2)te_2b_2 + (2x_0x_3 + 2x_1x_2)b_2 = 0\\
&h_3 : -2Xte_3^3 - 2te_3X - Yte_3^4 + Y + (2x_0x_3 + 2x_1x_2)\\
&\quad b_3te_3^4 + 4(x_1^2 - x_2^2)b_3te_3^3 + (4x_0x_3 - 12x_1x_2)b_3te_3^2\\
&\quad - 4(x_1^2 - x_2^2)te_3b_3 + (2x_0x_3 + 2x_1x_2)b_3 = 0
\end{aligned} \quad (15)$$

Then these three constraint equations are written as a polynomial ideal $\mathcal{I} = \langle h_1, h_2, h_3\rangle$ with variables $\{x_0, x_1, x_2, x_3, X, Y\}$ over the coefficient ring $\mathbb{C}[b_1, b_2, b_3, te_2, te_3]$. The primary decomposition is computed and it turns out that $\mathcal{I}$ cannot be decomposed, but it can be reformulated as $\mathcal{I} = \langle g_1, g_2, g_3\rangle$:

$$\begin{aligned}
g_1 : &(2b_2te_2^3te_3^3 - 2b_3te_2^3te_3^3 + 2b_2te_2^3te_3 - 2b_2te_2te_3^3 + 2\\
&b_3te_2^3te_3 - 2b_3te_2te_3^3 - 2b_2te_2te_3 + 2b_3te_2te_3)x_1^2 + (\\
&b_1te_2^4te_3^3 - b_1te_2^3te_3^4 + b_2te_2^4te_3^3 - b_3te_2^3te_3^4 + b_1te_2^4te_3\\
&- b_1te_2te_3^4 + b_2te_2^4te_3 - 6b_2te_2^2te_3^3 + 6b_3te_2^3te_3^2 - b_3\\
&te_2te_3^4 + b_1te_2^3 - b_1te_3^3 - 6b_2te_2^2te_3 + b_2te_3^3 - b_3te_2^3 +\\
&6b_3te_2te_3^2 + b_1te_2 - b_1te_3 + b_2te_3 - b_3te_2)x_1x_2 + (-\\
&2b_2te_2^3te_3^3 + 2b_3te_2^3te_3^3 - 2b_2te_2^3te_3 + 2b_2te_2te_3^3 - 2b_3\\
&te_2^3te_3 + 2b_3te_2te_3^3 + 2b_2te_2te_3 - 2b_3te_2te_3)x_2^2 + (b_1\\
&te_2^4te_3^3 - b_3te_2^3 - b_1te_2^3te_3^4 + b_2te_2^4te_3^3 - b_3te_2^3te_3^4 + b_1\\
&te_2^4te_3 - b_1te_2te_3^4 + b_2te_2^4te_3 + b_2te_3^3 + 2b_2te_2^2te_3^3 - 2\\
&b_3te_2^3te_3^2 - b_3te_2te_3^4 + b_1te_2^3 - b_1te_3^3 + 2b_2te_2^2te_3 + b_1\\
&te_2 - b_1te_3 + b_2te_3 - b_3te_2 - 2b_3te_2te_3^2)x_0x_3 = 0
\end{aligned} \quad (16)$$

$$\begin{aligned}
g_2 : &Y(b_1te_2^4te_3^3 - b_1te_2^3te_3^4 + b_2te_2^4te_3^3 - b_3te_2^3te_3^4 + b_1\\
&te_2^4te_3 - b_1te_2te_3^4 - b_3te_2 + b_2te_2^4te_3 + 2b_2te_2^2te_3^3\\
&- 2b_3te_2^3te_3^2 - b_3te_2te_3^4 + b_1te_2^3 - b_1te_3^3 + b_2te_3\\
&+ 2b_2te_2^2te_3 + b_2te_3^3 - b_3te_2^3 - 2b_3te_2te_3^2 + b_1te_2\\
&- b_1te_3) + (-4b_1b_2te_2^3te_3^3 + 4b_1b_3te_2^3te_3^3 - 4b_1b_2\\
&te_2^3te_3 + 4b_1b_2te_2te_3^3 - 4b_1b_3te_2^3te_3 + 4b_1b_3te_2te_3^3\\
&+ 4b_1b_2te_2te_3 - 4b_1b_3te_2te_3)x_1^2 + (16b_1b_2te_2^2te_3^3\\
&- 16b_1b_3te_2^3te_3^2 + 16b_1b_2te_2^2te_3 - 16b_1b_3te_2te_3^2)\\
&x_1x_2 + (4b_1b_2te_2^3te_3^3 - 4b_1b_3te_2^3te_3^3 + 4b_1b_2te_2^3te_3\\
&- 4b_1b_2te_2te_3^3 + 4b_1b_3te_2^3te_3 - 4b_1b_3te_2te_3^3 - 4\\
&b_1b_2te_2te_3 + 4b_1b_3te_2te_3)x_2^2 = 0
\end{aligned} \quad (17)$$

$$\begin{aligned}
g_3 : &X(b_1te_2^4te_3^3 - b_1te_2^3te_3^4 + b_2te_2^4te_3^3 - b_3te_2^3te_3^4 + b_1\\
&te_2^4te_3 - b_1te_2te_3^4 + b_2te_2^4te_3 + 2b_2te_2^2te_3^3 - 2b_3te_2^3\\
&te_3^2 - b_3te_2te_3^4 + b_1te_2^3 - b_1te_3^3 - b_3te_2 + 2b_2te_2^2te_3\\
&+ b_2te_3^3 - b_3te_2^3 - 2b_3te_2te_3^2 + b_1te_2 - b_1te_3 + b_2\\
&te_3) + (2b_1b_2te_2^3te_3^4 - 2b_1b_3te_2^4te_3^3 - 2b_2b_3te_2^4te_3^3 +\\
&2b_2b_3te_2^3te_3^4 - 2b_1b_2te_2te_3^4 + 2b_1b_3te_2^4te_3 + 2b_2b_3\\
&te_2^4te_3 + 4b_2b_3te_2^3te_3^2 - 4b_2b_3te_2^2te_3^3 - 2b_2b_3te_2te_3^4\\
&- 2b_1b_2te_2^3 + 2b_1b_3te_3^3 + 2b_2b_3te_2^3 + 4b_2b_3te_2^2te_3 -\\
&4b_2b_3te_2te_3^2 - 2b_2b_3te_3^3 + 2b_1b_2te_2 - 2b_1b_3te_3 - 2\\
&b_2b_3te_2 + 2b_2b_3te_3)x_1^2 + (-8b_1b_2te_2^2te_3^4 + 8b_1b_3te_2^4\\
&te_3^2 + 8b_2b_3te_2^4te_3^2 - 8b_2b_3te_2^2te_3^4 + 8b_1b_2te_2^2 - 8b_1\\
&b_3te_3^2 - 8b_2b3te_2^2 + 8b_2b_3te_3^2)x_1x_2 + (-2b_1b_2te_2^3\\
&te_3^4 + 2b_1b_3te_2^4te_3^3 + 2b_2b_3te_2^4te_3^3 - 2b_2b_3te_2^3te_3^4 +
\end{aligned} \quad (18)$$

$$2b_1b_2te_2te_3^4 - 2b_1b_3te_2^4te_3 - 2b_2b_3te_2^4te_3 - 4b_2b_3 te_2^3te_3^2 + 4b_2b_3te_2^2te_3^3 + 2b_2b_3te_2te_3^4 + 2b_1b_2te_2^3 - 2b_1b_3te_3^3 - 2b_2b_3te_2^3 - 4b_2b_3te_2^2te_3 + 4b_2b_3te_2te_3^2 + 2b_2b_3te_3^3 - 2b_1b_2te_2 + 2b_1b_3te_3 + 2b_2b_3te_2 - 2b_2b_3te_3)x_2^2 = 0$$

It can be seen from Eqs. (16-18) that g_1, g_2, g_3 are free of Z component. This means that for any value of the design parameters $(b_1, b_2, b_3, \varepsilon_2, \varepsilon_3)$, the manipulator can always perform a pure translation along **z** direction.

Variable x_3 can be solved linearly from g_1 and x_3 is parametrized by x_0, x_1, x_2. This means that the manipulator is capable of orientations determined by x_0, x_1, x_2 in which variable x_3 is not null. The mechanism might be subjected to a parasitic motion as discussed in [25], [26].

The equations g_2, g_3 can be solved linearly for variables Y and X, respectively. This shows that the manipulator undergoes translational motions along **x** and **y** directions which are coupled to the orientations. In the following, the rotational components $\{x_0, x_1, x_2, x_3\}$ from g_1, g_2, g_3 are constrained to be equal to zero, which leads to different operation modes. By fulfilling this condition, the design parameters are synthesized and new architectures are proposed.

A.1 Case $x_0 = 0$

One variable is constrained to be null, namely $x_0 = 0$. Since only the equation g_1 has component x_0, the computation will be carried out only for g_1. After substituting $x_0 = 0$, equation g_1 becomes:

$$g_1 : ax_1^2 + bx_1x_2 + cx_2^2 = 0 \tag{19}$$

where a, b, c are polynomial coefficients in terms of the design parameters $(b_1, b_2, b_3, te_2, te_3)$.

To synthesize the design parameters, all polynomial coefficients have to vanish. Hence, one has to discuss the ideal $\mathcal{J} = \langle a, b, c\rangle$. The Groebner basis of the ideal $\mathcal{J}$ with lexicographic order is computed and 17 solutions are obtained for the design parameters. Not all solutions are possible and hence some assumptions are made, as follows:

1. The second and the third legs cannot be coincident with the first leg:
- $\varepsilon_2 \neq 0$ and $\varepsilon_3 \neq 0$
2. The second leg cannot be coincident with the third leg:
- $\varepsilon_2 \neq \varepsilon_3$
3. The magnitude of b_i $(i = 1, 2, 3)$ should be positive:
- $b_i \geq 0, i = 1, 2, 3$
4. The platform cannot be a point:
- $b_1 \neq b_2 \neq b_3 \neq 0$
5. No complex solutions:
- $\{b_1, b_2, b_3, \varepsilon_2, \varepsilon_3\} \in \mathbb{R}$

After removing the solutions that do not fulfil the assumptions stated above, four designs are obtained:

$$\begin{aligned}
&L_1 : b_2 = 0, b_3 = 0, \varepsilon_3 = \pi + \varepsilon_2 \\
&L_2 : b_2 = \frac{b_1}{\tan(\varepsilon_3)}, b_3 = 0, \varepsilon_2 = \frac{\pi}{2}, \varepsilon_3 \neq 0 \text{ or } \varepsilon_3 \neq \pm\pi \\
&L_3 : b_2 = -\frac{b_1}{\tan(\varepsilon_3)}, b_3 = 0, \varepsilon_2 = -\frac{\pi}{2}, \varepsilon_3 \neq 0 \text{ or } \varepsilon_3 \neq \pm\pi \\
&L_4 : b_1 = b_3\frac{\cos(\varepsilon_2 - \varepsilon_3)}{\cos(\varepsilon_2)}, b_2 = b_3\frac{\cos(\varepsilon_3)}{\cos(\varepsilon_2)}, \varepsilon_2 \neq \pm\frac{\pi}{2} \text{ or } \\
&\quad \varepsilon_2 \neq \pm\frac{3\pi}{2}
\end{aligned} \tag{20}$$

The 3-RPS parallel manipulator can be generated by selecting one of the designs (L_1, L_2, L_3, L_4). In the following, the parallel manipulators obtained with designs L_2 and L_4 are presented.

Design L_2

In design L_2, some values are assigned as $b_1 = 1$ and $\varepsilon_3 = -2\pi/3$. Other design parameters are obtained as: $b_2 = \sqrt{3}/3, b_3 = 0, \varepsilon_2 = \pi/2$. The new architecture of the 3-RPS manipulator is depicted in Fig. 3. The base and the moving platform have right-angle triangle shapes. The unit vectors $\mathbf{s}_1$ and $\mathbf{s}_2$ are orthogonal ($\mathbf{s}_1 \perp \mathbf{s}_2$).

The values of the design parameters are substituted into the set of three constraint equations defined in Eq. (13). Then the constraint equations associated with the new parallel manipulator are:

$$\begin{aligned}
&k_1 : Y + 2x_0x_3 + 2x_1x_2 \\
&k_2 : 2\sqrt{3}x_0x_3 - 2\sqrt{3}x_1x_2 - 3X \\
&k_3 : X\sqrt{3} - Y
\end{aligned} \tag{21}$$

These three constraint equations are defined as a new ideal $\mathcal{K} = \langle k_1, k_2, k_3\rangle$ and the primary decomposition is computed to verify if the ideal $\mathcal{K}$ is the intersection of several smaller ideals. Indeed, the ideal $\mathcal{K}$ is decomposed into two components, which correspond to two different operations modes as $\mathcal{K} = \bigcap_{i=1}^{2} \mathcal{K}_i$, with the results of primary decomposition:

$$\begin{aligned}
\mathcal{K}_1 &= \langle x_0, 3X - \sqrt{3}Y, 2x_1x_2 + Y\rangle \\
\mathcal{K}_2 &= \langle x_3, 3X - \sqrt{3}Y, 2x_1x_2 + Y\rangle
\end{aligned} \tag{22}$$

The first operation mode is shown by the first sub-ideal $\mathcal{K}_1$, in which $x_0 = 0$. All possible poses of the mechanism in this operation mode are obtained by rotating the platform from the home configuration about a transformation axis by π and translating along the same direction. The second operation mode is shown by the sub-ideal $\mathcal{K}_2$ with $x_3 = 0$. In this operation mode, the transformation axis is parallel to the **xy**-plane of Σ_0. The investigation of these two operation modes are discussed in more detail in [4].

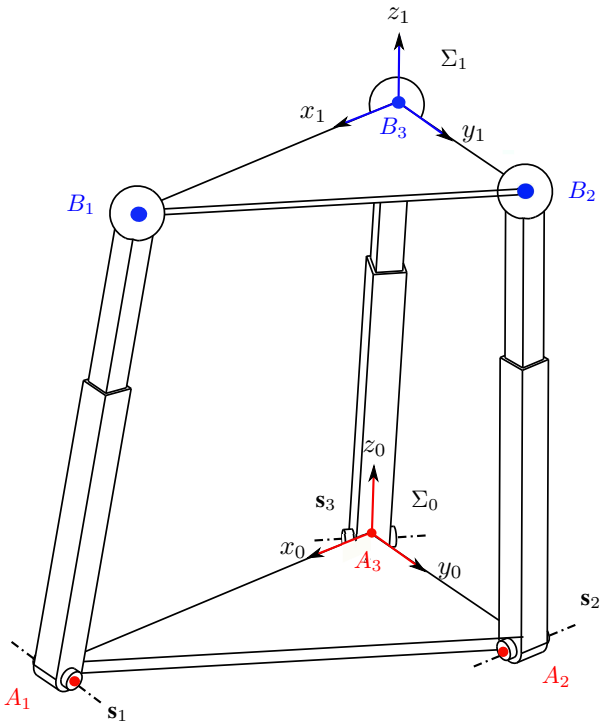

Fig. 3. The 3-RPS parallel manipulator based on design L_2.

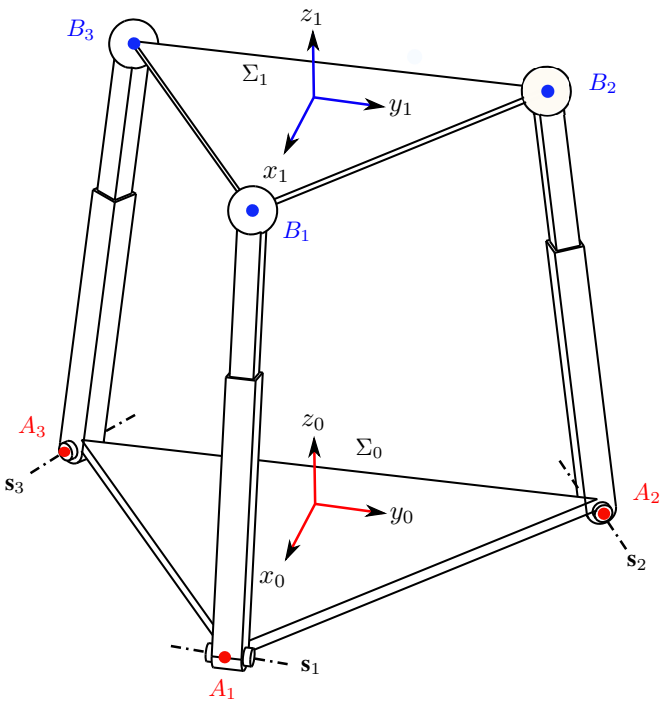

Fig. 4. The 3-RPS parallel manipulator based on design L_4.

Design L_4

In design L_4, the design parameters $b_3, \varepsilon_2, \varepsilon_3$ are assigned, namely $b_3 = 1$, $\varepsilon_2 = \frac{2\pi}{3}$, and $\varepsilon_3 = -\frac{2\pi}{3}$. Therefore, we can obtain $b_1 = 1$ and $b_2 = 1$. The 3-RPS parallel manipulator generated with these design parameters has the equilateral triangle base and the equilateral triangle platform, as depicted in Fig. 4. This 3-RPS parallel manipulator was introduced by Hunt in 1983 [1].

The set of three constraint equations in Eq. (13) is recalled and the values of the design parameters are substituted. This yields:

$$\begin{aligned} k_1 &: Y + 2x_0x_3 + 2x_1x_2 \\ k_2 &: \sqrt{3}x_1^2 - \sqrt{3}x_2^2 - \sqrt{3}X + 4x_0x_3 - 2x_1x_2 - Y \\ k_3 &: -\sqrt{3}x_1^2 + \sqrt{3}x_2^2 + \sqrt{3}X + 4x_0x_3 - 2x_1x_2 - Y \end{aligned} \tag{23}$$

These constraint equations are written as an ideal $\mathcal{K} = \langle k_1, k_2, k_3 \rangle$ and the primary decomposition is computed. It turns out that the ideal $\mathcal{K}$ is decomposed into two components, which correspond to two different operations modes as $\mathcal{K} = \bigcap_{i=1}^{2} \mathcal{K}_i$, with the results of primary decomposition:

$$\begin{aligned} \mathcal{K}_1 &= \langle x_0, -x_1^2 + x_2^2 + X, 2x_1x_2 + Y \rangle \\ \mathcal{K}_2 &= \langle x_3, -x_1^2 + x_2^2 + X, 2x_1x_2 + Y \rangle \end{aligned} \tag{24}$$

It turns out that the manipulators generated by either design L_2 or design L_4 will have similar number and type of operation modes, namely $x_0 = 0$ and $x_3 = 0$. This condition is applied also for other designs, namely L_1 and L_3. However, they might have different parasitic motions o f translations in **x** and **y** directions.

A.2 Case $x_3 = 0$

In this section, variable x_3 is constrained to be equal to null. In Eqs. (16-18), only the equation g_1 has variable x_3. In equation g_1, only one monomial contains variable x_3 and apparently this monomial contains variable x_0 simultaneously.

Accordingly, the synthesis of the design parameters with $x_3 = 0$ will lead to the same designs as determined in Section V-A.1, namely Eq. 20. This means that the 3-RPS manipulators generated in this section will have at least two operation modes containing $x_0 = 0$ and $x_3 = 0$.

A.3 Case $x_1 = 0$

In this section, the variable x_1 in Eqs. (16-18) is constrained to be null. After substituting $x_1 = 0$, the equations g_1, g_2, g_3 become:

$$\begin{aligned} g_1 &: \; ax_0x_3 + bx_2^2 = 0 \\ g_2 &: \; cY + dx_2^2 = 0 \\ g_3 &: \; eX + fx_2^2 = 0 \end{aligned} \tag{25}$$

where a, b, c, d, e, f are polynomial coefficients in terms of the design parameters $(b_1, b_2, b_3, te_2, te_3)$.

To synthesize the design parameters corresponding to the variable $x_1 = 0$, all polynomial coefficients in Eq. (25)

have to vanish. Accordingly, one has to discuss the ideal $\mathcal{J} = \langle a, b, c, d, e, f \rangle$. The Groebner basis of ideal $\mathcal{J}$ with lexicographic order is computed and 11 solutions of the design parameters are obtained. Not all solutions are possible and hence by following the aforementioned assumptions in Section V-A.1, three designs are obtained as:

$$
\begin{aligned}
&L_1 : b_2 = -\frac{b_1}{\tan(\varepsilon_3)}, b_3 = 0, \varepsilon_2 = \frac{\pi}{2}, \varepsilon_3 \neq 0 \text{ or } \varepsilon_3 \neq \pm\pi \\
&L_2 : b_2 = \frac{b_1}{\tan(\varepsilon_3)}, b_3 = 0, \varepsilon_2 = -\frac{\pi}{2}, \varepsilon_3 \neq 0 \text{ or } \varepsilon_3 \neq \pm\pi \\
&L_3 : b_1 = -b_3\frac{\cos(\varepsilon_2 - \varepsilon_3)}{\cos(\varepsilon_2)}, b_2 = b_3\frac{\cos(\varepsilon_3)}{\cos(\varepsilon_2)}, \varepsilon_2 \neq \pm\frac{\pi}{2} \\
&\quad \text{or } \varepsilon_2 \neq \pm\frac{3\pi}{2}
\end{aligned}
\tag{26}
$$

By selecting one of the designs (L_1, L_2, L_3), a new 3-RPS parallel manipulator can be built. The application of the design L_3 is presented in the following.

Design L_3

Design L_3 is selected to generate the 3-RPS parallel manipulator whose operation modes contain $x_1 = 0$. The design parameters $b_3 = 1$, $\varepsilon_2 = \pi/4$, and $\varepsilon_3 = -\pi/4$ are assigned, hence $b_1 = \sqrt{2}$ and $b_2 = 1$ are determined. The 3-RPS parallel manipulator with these design parameters is depicted in Fig. 5, in which the base and the moving platform have right-angle triangle shapes. The axes of the second and the third revolute joints are orthogonal and meet at point A_1.

The values of the design parameters are substituted into the set of three constraint equations defined in Eq. (13). Then the constraint equations associated with the new parallel manipulator are:

$$
\begin{aligned}
k_1 &: Y + 2\sqrt{2}x_0x_3 + 2\sqrt{2}x_1x_2 \\
k_2 &: -\sqrt{2}X + \sqrt{2}Y + 4x_0x_3 - 2x_1^2 + 2x_2^2 \\
k_3 &: \sqrt{2}X + \sqrt{2}Y + 4x_0x_3 + 2x_1^2 - 2x_2^2
\end{aligned}
\tag{27}
$$

These three constraint equations are defined as a new ideal $\mathcal{K} = \langle k_1, k_2, k_3 \rangle$ and the primary decomposition is computed to verify if the ideal $\mathcal{K}$ is the intersection of several smaller ideals. Indeed, the ideal $\mathcal{K}$ is decomposed into two components, which correspond to two different operations modes as $\mathcal{K} = \bigcap_{i=1}^{2} \mathcal{K}_i$, with the results of primary decomposition:

$$
\begin{aligned}
\mathcal{K}_1 &= \langle x_1, 4x_0x_3 + \sqrt{2}Y, 2x_2^2 - \sqrt{2}X \rangle \\
\mathcal{K}_2 &= \langle x_2, 4x_0x_3 + \sqrt{2}Y, 2x_1^2 + \sqrt{2}X \rangle
\end{aligned}
\tag{28}
$$

The sub-ideal $\mathcal{K}_1$ shows the first operation mode of this manipulator, in which $x_1 = 0$. In this operation mode, the moving platform is transformed from the home configuration about an axis parallel to the **yz**-plane of Σ_0. The second operation mode of this manipulator is shown by sub-ideal $\mathcal{K}_2$ with $x_2 = 0$. The transformation axis of this operation mode is parallel to the **xz**-plane of Σ_0.

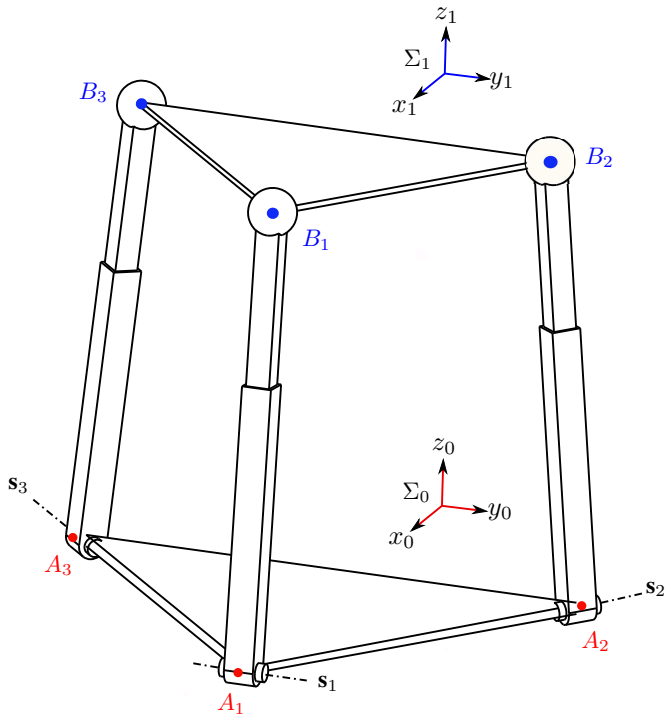

Fig. 5. The 3-RPS parallel manipulator based on design L_3.

A.4 Case $x_2 = 0$

In this section, variable x_2 is constrained to be equal to zero. Substituting $x_2 = 0$ into Eqs. (16-18), we obtain:

$$
\begin{aligned}
g_1 &: \; ax_0x_3 + bx_1^2 = 0 \\
g_2 &: \; cY + dx_1^2 = 0 \\
g_3 &: \; eX + fx_1^2 = 0
\end{aligned}
\tag{29}
$$

where a, b, c, d, e, f are polynomial coefficients in terms of the design parameters $(b_1, b_2, b_3, te_2, te_3)$.

It turns out that the polynomial coefficients in Eq. (29) have the same mathematical expressions as the polynomial coefficients in Eq. (25). The computation yields three designs, which are identical to Eq. (26) derived in Section V-A.3. Eventually one can conclude that the 3-RPS parallel manipulators generated in this section will have at least two operation modes containing $x_1 = 0$ and $x_2 = 0$.

VI. Conclusions

In this paper, the synthesis of the design parameters corresponding to the prescribed operation modes for a parallel manipulator with three RPS legs was addressed. The Euler parametrization and the results of primary decomposition were used to define the synthesis procedure by considering the type and number of operation modes at the design stage.

First, the parametrization of one RPS leg was defined. Then, the constraint equation corresponding to this leg was derived. Accordingly, seven classes of the RPS legs were obtained. Each class contains several sub-classes corresponding to the specific position and orientation of the RPS legs.

As a result, it is possible to generate new 3-RPS parallel manipulator architectures by selecting three different or identical classes of RPS legs. The constraint equations of the new manipulators have been formulated and the corresponding primary decomposition has been computed.

In the results of primary decomposition, some constraints were applied to the Euler parameters that lead to particular types of operation modes. The polynomial coefficients of the results of primary decomposition depend on the design parameters. Consequently, the design parameters were synthesized by computing the Groebner basis over an ideal of these polynomial coefficients. Several architectures of the 3-RPS parallel manipulators corresponding to the prescribed operation modes were presented. The applications of the proposed approach for parallel manipulators with different types of legs will be the subject of future research.

References

[1] Hunt K. H. Structural Kinematics of In-Parallel-Actuated Robot-Arms. *ASME Journal of Mechanisms, Transmissions, and Automation in Design*, 105(67):705–712, 1983.

[2] Huang Z., Wang J., and Fang Y. Analysis of Instantaneous Motions of Deficient Rank 3-RPS Parallel Manipulators. *Mechanism and Machine Theory*, 27:229–240, 2002.

[3] Lung-Wen Tsai. *Robot Analysis: The Mechanics of Serial and Parallel Manipulators.*. John Wiley & Sons Inc, 1999.

[4] Schadlbauer J., Walter D. R., and Husty M. L. The 3-RPS Parallel Manipulator from an Algebraic Viewpoint. *Mechanism and Machine Theory*, 75:161–176, 2014.

[5] Schadlbauer J., Nurahmi L., Husty M., Wenger P., and Caro S. Operation Modes in Lower Mobility Parallel Manipulators. *Interdisciplinary Applications of Kinematics, Andres Kecskemetthy and Francisco Geu Flores (Eds.)*, 26:1–9, 2015.

[6] Schadlbauer J., Husty L., Caro S., and Wenger P. Self-motions of 3-RPS Manipulators. *Journal of Frontiers of Mechanical Engineering*, 8(1):62–69, 2013.

[7] Han Sung Kim and Lung-Wen Tsai. Kinematic Synthesis of a Spatial 3-RPS Parallel Manipulator. *ASME Journal of Mechanical Design*, 125(1):92–97, 2003.

[8] Nalluri Mohan Rao and Mallikarjuna Rao K. Multi-position Dimensional Synthesis of a Spatial 3-RPS Parallel Manipulator. *ASME Journal of Mechanical Design*, 128(4):815–819, 2006.

[9] Nalluri Mohan Rao and Mallikarjuna Rao K. Dimensional Synthesis of a Spatial 3-RPS Parallel Manipulator for a Prescribed Range of Motion of Spherical Joints. *Mechanism and Machine Theory*, 44(22):477–486, 2009.

[10] Huang Z. and Fang Y. Motion Characteristics and Rotational Axis Analysis of Three DOF Parallel Robot Mechanisms. In *IEEE Int. Conf. on Systems, Man, and Cybernetics*, pp. 67–71, 1995.

[11] Huang Z., Chen Z., Liu J., and Liu S. A 3 DOF Rotational Parallel Manipulator Without Intersecting Axes. *ASME Journal Mechanisms and Robotics*, 3(2):1–8, 2011.

[12] Chen Z., Cao W-A., and Huang Z. Type Synthesis of 3-DOF Rotational Parallel Mechanisms With No Intersecting Axes. In *ASME International Design Engineering Technical Conferences and Computers & Information in Engineering Conference*, pp. 565–572, Chicago, USA, 2012.

[13] Zhen Huang, Dejun Mu, and Daxing Zeng. The Screw Motion Simulation on 3-RPS Parallel Pyramid Mechanism. In *IEEE Int. Conf. on Mechatronics and Automation*, pp. 2860–2864, Harbin, Heilongjiang, China, August 5-8, 2007.

[14] Nurahmi L., Schadlbauer J., Husty M., Caro S., and Wenger P. Kinematic Analysis of the 3-RPS Cube Parallel Manipulator. *ASME Journal Mechanisms and Robotics*, 7(1):0110081-01100811, 2015.

[15] Nurahmi L., Schadlbauer J., Husty M., Wenger P., and Caro S. Kinematic Analysis of the 3-RPS Cube Parallel Manipulator. In *ASME International Design Engineering Technical Conferences and Computers & Information in Engineering Conference*, Buffalo, New York, USA, August 17-20, 2014.

[16] Nurahmi L., Schadlbauer J., Husty M., Wenger P., and Caro S. Motion Capability of the 3-RPS Cube Parallel Manipulator. In *Advances in Robot Kinematics, Jadran Lenarcic and Oussama Khatib (Eds.)*, 527–535, 2014.

[17] Shaoping Bai and Stéphane Caro. Design and Analysis of a 3-PPR Planar Robot with U-shape Base. In *Proceedings of the 14th International Conference on Advanced Robotics*, Munich, Germany, June 22-26, 2009.

[18] Bottema O. and Roth B. *Theoretical Kinematics.*. Dover Publications, New York, 1990.

[19] Nurahmi L., Caro S., and Wenger P. Operation Modes and Self-motions of a 2-RUU Parallel Manipulator. *Recent Advances in Mechanism Design for Robotics, Marco Ceccarelli and Shaoping Bai (Eds.)*, 33:417–426, 2015.

[20] Xianwen Kong. Reconfiguration Analysis of a 3-DOF Parallel Mechanism Using Euler Parameter Quaternions and Algebraic Geometry Method. *Mechanism and Machine Theory*, 74:188–201, 2014.

[21] Walter D.R., Husty M.L., and Pfurner M. A Complete Kinematic Analysis of the SNU 3-UPU Parallel Robot. *Contemporary Mathematics*, 496:331–346, 2009.

[22] Walter D.R. and Husty M.L. Kinematic Analysis of the TSAI 3-UPU Parallel Manipulator Using Algebraic Methods. In *IFToMM 13th World Congress in Mechanism and Machine Science*, pp. 19-25, Mexico, June 19-23, 2011.

[23] http://www.irccyn.ec-nantes.fr/%7enurahmi/IFToMM2015/App.pdf

[24] Husty M.L., Pfurner M., Shrocker H.-P., and Brunnthaler K. Algebraic Methods in Mechanism Analysis and Synthesis. *Robotica*, 25(06):661–675, 2007.

[25] Carretero J.A., Podhoredeski R.P., Nahon M.A., and Gosselin C.M. Kinematic Analysis and Optimization of a New Three Degree-ofFreedom Spatial Parallel Manipulator. *ASME Journal of Mechanical Design*, 122:17-24, 2000.

[26] Li Q., Chen Z., Chen Q., Wu C., and Hu X. Parasitic Motion Comparison of 3-PRS Parallel Mechanism with Different Limb Arrangements. *Robotics and Computer-Integrated Manufacturing*, 27(2):389-396, 2011.